

Temperature-dependent surface morphologies for Br-etched Si(100)-2×1

D. Rioux, R. J. Pechman, M. Chander, and J. H. Weaver

Department of Materials Science and Chemical Engineering, University of Minnesota, Minneapolis, Minnesota 55455

(Received 22 April 1994)

Temperature-dependent surface morphologies resulting from spontaneous Br etching of Si(100)-2×1 in the range 600–1100 K have been studied using scanning tunneling microscopy. The etch pits and Si structures on the exposed surfaces exhibit temperature-dependent shape, size, and distribution characteristics. Although the morphology depends on temperature, the steady-state removal of Si is dominated by layer-by-layer etching that produces bounded surface roughness. Temperature-dependent kinetics, surface reactivities, and product evolution are responsible for the different morphologies.

INTRODUCTION

Plasma etching is important in device processing and manufacturing, particularly since electronic-device dimensions continue to shrink.^{1,2} In such complex systems, basic research has the opportunity to provide important insights. For example, improved understanding of phenomena associated with plasma reactions using halogenated feed gases can be achieved by studying simple halogen-semiconductor model systems. Halogen-surface interactions include so-called spontaneous etching that is associated with the thermally activated formation of volatile species. More complex interactions can involve electron, ion, or photon activation.²

Surface-layer removal by etching can be considered as the inverse process to surface-layer growth, and some of the vocabulary of epitaxial growth can be used to describe etching. For example, Patrin and co-workers^{3,4} used scanning tunneling microscopy (STM) to investigate Br and Cl etching of GaAs(110), and they noted that surface morphologies depended on etching variables in a manner similar to the growth process. They found that rougher surfaces were formed as the etchant flux was increased, although the material was removed in a layer-by-layer fashion. Boland and Villarrubia⁵ examined Cl₂ interactions with Si(111)-7×7 and demonstrated that most of the adatom layer was stripped away to reveal the underlying Si rest-atom layer when a Cl-saturated surface was annealed. Chander *et al.*⁶ reported bounded etching for continuous exposure of Si(100)-2×1 to Br₂ at 900 K, and Rioux *et al.*⁷ demonstrated that the etchant arrival rate affected the surface morphology during the initial stages of etching.

In this paper, we further examine the analogy to epitaxial growth and show that the steady-state morphologies for Br-etched Si(100)-2×1 are temperature dependent. Analysis of STM images of post-etch surfaces, in combination with temperature programmed desorption (TPD) data,⁸ demonstrates that this dependence results from thermally-activated etch channels and temperature-dependent kinetics. TPD shows that SiBr₃ and SiBr₄ are the dominant desorption products at low temperatures but that SiBr₂ becomes favored at higher temperatures. Consequently, etch rates depend strongly on temperature, and they can be controlled under condi-

tions of constant flux. Temperature dependencies are also evident in the diffusion of Si on the surface and the diffusion of vacancies created by etching, effects that can be related to the observed structural variations in steady-state etching. The goal of the present work, then, was to formulate a coherent picture of layer-by-layer Br etching as a function of temperature, flux, and fluence.

EXPERIMENT

The experiments were performed in an ultrahigh vacuum chamber equipped with a Park Scientific Instruments STM. The base pressure of the system was 5×10^{-11} Torr. Silicon wafers oriented within 0.2° – 0.5° of (100) and miscut toward [110] were rinsed in ethanol prior to introduction into vacuum. The wafers were degassed at 600°C for several hours and flashed to 1200°C for 1–2 min. This procedure produces clean, well-ordered Si(100)-2×1.⁹ Sample temperatures, which ranged from 600–1100 K during exposure to Br₂, were monitored with an optical pyrometer. They were accurate to within ± 20 K and were reproducible to ± 5 K. Electrochemically-etched tungsten tips were cleaned using electron bombardment. Scan dimensions were calibrated with the lattice constant of the Si(100)-2×1 surface and the height of monatomic steps. All STM micrographs were acquired in a constant current mode at room temperature. Some images show slight distortions because they were not corrected for thermal drift of the scanner.

An electrochemical cell¹⁰ consisting of a AgBr pellet doped with CdBr₂ was used to provide molecular bromine for dosing. An applied voltage caused halogen ions to diffuse to a Pt mesh electrode where they combined and desorbed as Br₂. The sample was ~ 3 cm from the mesh electrode during exposures. During operation of the cell the chamber pressure remained below 1×10^{-10} Torr. Stable cell currents of 10–15 μ A were used, releasing a flux of $\sim 3.2 \times 10^{13}$ to $\sim 4.8 \times 10^{13}$ Br₂ molecules per second. Bromine exposures were done under conditions of constant flux for predetermined amounts of time so that exposures are quoted as a fluence in units of mA s. The sample was cooled rapidly to room temperature immediately upon terminating the flux. We note that the halogen flux incident on the sample depends on the experimental geometry and that sticking depends on sur-

face conditions and temperature. The temperature-dependent sticking coefficient renders the absolute Br uptake uncertain, so we avoid comparing morphologies at equivalent fluences for samples etched at different temperatures. While we contrast surfaces at equivalent stages of etching, we also quote fluences for completeness. The steady-state surface conditions at each temperature were determined by exposures that were sufficiently long to assure that the morphology did not undergo subsequent changes. This was verified experimentally by studies as a function of fluence.

STEADY-STATE ETCHING

A. Overview

Temperature programmed desorption studies of the interaction of Br with Si(100)- 2×1 have shown that two adsorption states, termed α and β , exist with desorption peak temperatures above room temperature.⁸ The α state desorbs in the range ~ 350 – 700 K and the volatile species are primarily SiBr_3 and SiBr_4 . The β state desorbs in the range ~ 750 – 1100 K and is dominated by SiBr_2 . Isothermal analysis has demonstrated that the rate of halide evolution increases with temperature and is enhanced at the threshold temperatures for each adsorption state.⁸ The effect of temperature, then, is to facilitate the formation of bonding configurations that are unstable against desorption. At low temperature, only the Br-rich species are volatile but they are difficult to form. At high temperature, the backbonds are weakened, the less rich species are more readily formed, and they are volatile. The utility of STM is that it makes it possible to relate desorption profiles to atomic scale surface morphologies following etching at temperatures above and below the critical thresholds.

Figures 1–4 display constant current images from surfaces that have reached steady-state conditions for continuous etching at $600 \leq T \leq 1100$ K. Inspection reveals that the specific morphologies depend on temperature but that there are common temperature-independent structures present on most surfaces. These include one-dimensional chains (C) and two-dimensional islands (I) that form on the terraces. There are also single-layer deep etch pits (P) consisting of missing dimer rows and more extended vacancy islands.

From Figs. 1–3, we see that the etch pits are elongated along the dimer row direction after etching at $T \leq 1000$ K. This shape anisotropy reflects the fact that the single-layer deep etch pits are bounded by monatomic steps corresponding to S_A and S_B steps, as for the clean surface. Chander *et al.*⁶ related the preferential removal of Si along the dimer row direction to the difference in S_A and S_B step formation energies. Etching at 1100 K [Figs. 3(b) and 4(b)] is characterized by a unique effect in which the terrace vacancies interact to create line defects that are elongated perpendicular to the dimer rows, establishing an extended network in the steady state. Line defects will be discussed in detail in Section D.

High-resolution images indicate that atoms within the etch pits reconstruct to form 2×1 dimer rows that run

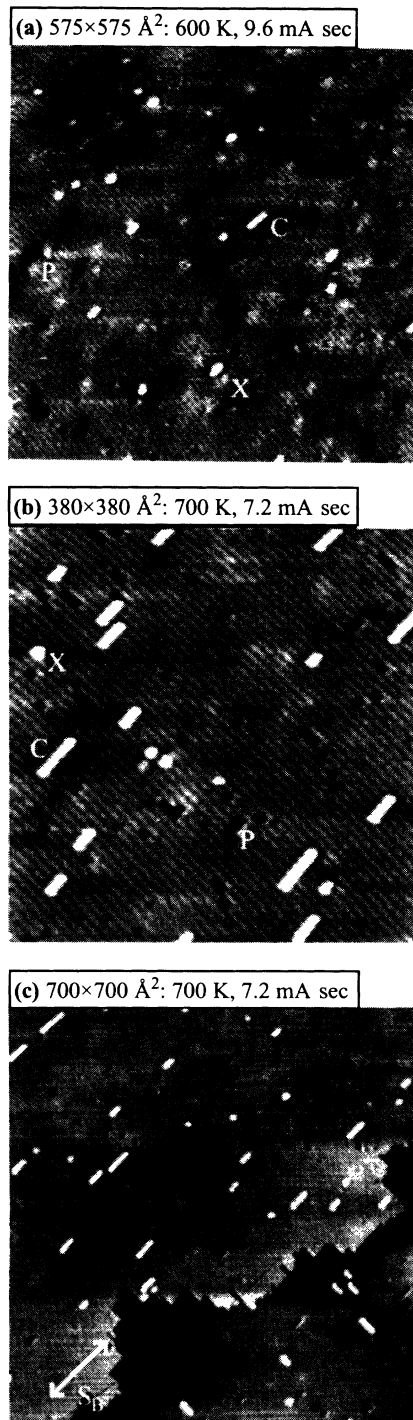


FIG. 1. Occupied states images of Si(100)- 2×1 exposed to Br_2 at (a) 600 K and (b), (c) 700 K. The images represent steady-state conditions in that they do not change in overall appearance with further exposure. The number and size of dimer chains (C) and anisotropic single-layer etch pits (P) increase with increasing temperature. The bright structureless features (X) may represent nonvolatile silicon bromide species. In (c) an S_B step edge crosses the image. Analysis indicates that such steps are roughened during etching but the terraces remain relatively defect free. Hence, etching is dominated by a step flow mechanism at 600 and 700 K. In this temperature region, desorption species are predominantly SiBr_3 and SiBr_4 .

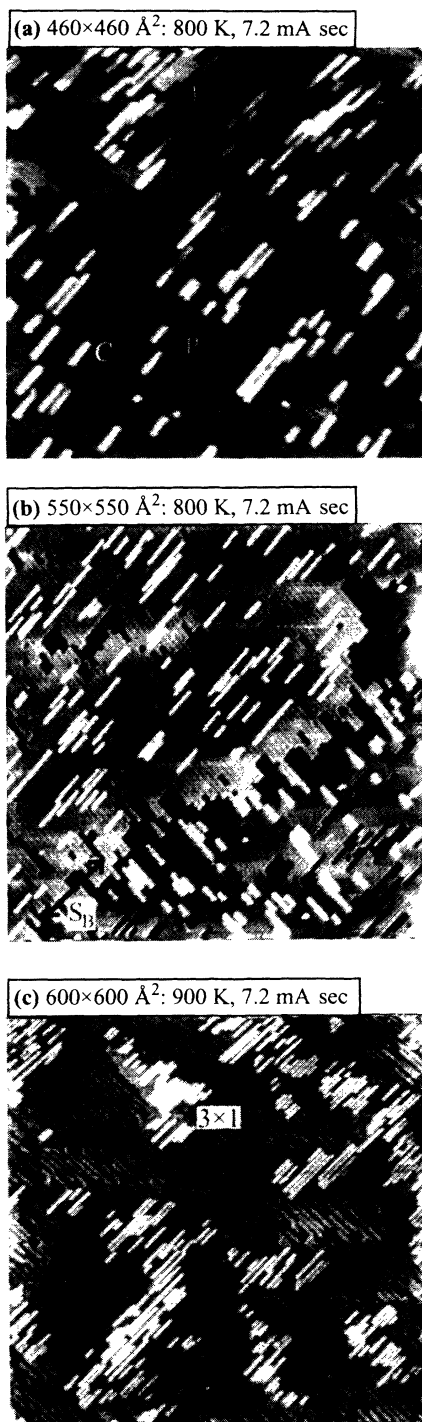


FIG. 2. Occupied states images of Si(100)- 2×1 exposed to Br_2 at (a), (b) 800 K and (c) 900 K. At 800 K a pathway involving SiBr_2 desorption is activated and this increases the etch rate. The result is enhanced terrace etching and rougher step edges. Step roughening occurs through facile material removal and Si regrowth near step edges. Etching also proceeds by pit formation on terraces at 800 K. As pits expand and coalesce, remnants of the terrace create islands that nucleate regrowth. At 900 K, 3×1 domains are produced by a coordinated surface transformation that yields atom rows of SiBr_2 separated by Br-terminated dimer rows. The SiBr_2 rows are volatile and desorb spontaneously, leaving behind dimer rows separated by missing atom rows [see text].

perpendicular to those of the surrounding terrace, as for adjacent terraces on clean vicinal surfaces.¹¹ This dimerization stabilizes the newly-exposed layer and impedes multilayer etching and roughening. The chains and islands that appear on the terraces also exhibit a 2×1 reconstruction with elongation perpendicular to the dimer row direction of the underlying terrace, as in Si(100) homoepitaxy.¹²⁻¹⁴ Such growth structures in Si homoepitaxy, and by extension the dimer chains observed here, result from different accommodation coefficients for Si atoms impinging at S_A and S_B step edges.¹⁴ With increasing temperature, the trend is toward longer chains and larger islands, though these structures become disordered and fragmented at 1000 and 1100 K [Figs. 3 and 4]. Detailed analyses of dimer chain characteristics are presented in the second part of this paper.

Steps play an important role in surface layer etching because they act as accumulation sites for Br. Silicon

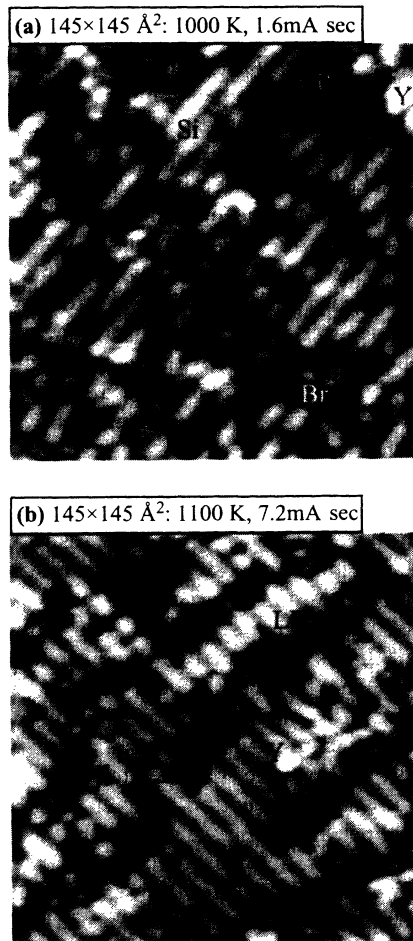


FIG. 3. Small-scale images taken after steady-state etching at (a) 1000 K and (b) 1100 K. (a) shows Br-free Si dimers (Si) and Br adsorption sites (Br) that are mixed with irregularly shaped pits (P). The bright feature labeled Y represents a disordered regrowth structure. (b) Dimer vacancies interact to form line defects (LD) that run perpendicular to the dimer row direction. Very little Br remains after etching at 1100 K and quenching to room temperature for imaging.

atoms along steps are thus more susceptible to removal than their terrace counterparts. In general, the step roughness increased with temperature up to 1000 K, as seen in Figs. 1, 2, and 4. Indeed, Figs. 2(c) and 4(a) show that steps are ill defined after steady-state etching at 900 and 1000 K. Analysis of step profiles in images such as these offers insight into the temperature-dependent etch mechanisms.

Inspection of many images like those in Figs. 1–4 suggests that the data can be categorized as representative of surfaces etched at low (LT), intermediate (IT), and high temperature (HT). The densities and shapes of the pits, chains, and islands depend on the temperature during Br exposure so that different steady-state morphologies are

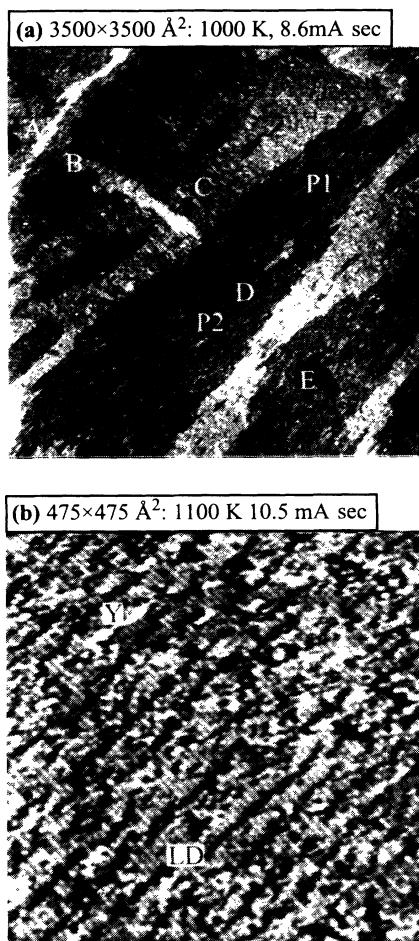


FIG. 4. Large-scale images taken after etching at (a) 1000 K and (b) 1100 K. (a) Five layers of Si are exposed by steady-state etching of a surface with 0.3–0.4- μm -wide terraces. Layers *A* and *B* are largely removed. Layer *C* dominates but large pits (*P1*) expose layer *D* and smaller pits (*P2*) expose layer *E*. This roughening is due to weakened Si-Si bonds and enhanced diffusion of Br. Surface defects are readily created and they facilitate terrace etching. (b) Etching at 1100 K produces a large number of vacancy defects. These defects are sufficiently mobile that they form networks of line defects. Roughly linear collections of bright features (*Y*) on terraces resemble regrowth structures, but the terrace disruption prevents the creation of ordered structures.

achieved. The term steady state is used here to denote an average surface structure that does not change with exposure. Though a particular feature may change its appearance, statistical populations and ensemble characteristics are not modified. Thus, steady-state morphologies represent a balance between etching, regrowth, and diffusion effects involving pits, islands, and step edges. The formation mechanisms of these structures depend on temperature, as described below.

B. Low-temperature (LT) etching at 600 and 700 K

The images in Fig. 1 represent surfaces etched at 600 and 700 K. They exhibit short 2×1 chains and small, single-layer etch pits that are distributed evenly on the terraces. High resolution scans of steady-state LT surfaces show that nearly all Si dangling bonds are satisfied by Br atoms, including those within pits and on chains, and that the 2×1 reconstruction is maintained. The presence of chemisorbed Br is determined from occupied state images in which Br-terminated dimers appear as two distinct atomic features.⁷ This is in contrast to results for clean Si(100)- 2×1 where equivalent images show single features with an elliptical shape.¹⁵

In general, the etch pits and terrace chains are only a few dimer units in size on surfaces etched at 600 and 700 K. Furthermore, the density of pits and chains is low and the chains remain isolated—features wider than two rows were not observed. Comparing Figs. 1(a) and 1(b) reveals an increased feature length and density at 70 K because of enhanced etching relative to 600 K. The low density and small size of the chains indicate that they reflect Si regrowth.

The intrinsic steps also exhibit changes due to etching. Figure 1(c) shows an S_B step from a surface etched at 700 K. Comparison of the step roughness to that for the starting surface demonstrates that the roughness increases, consistent with Si removal. Regrowth chains are equally distributed near S_A and S_B edges. This is in contrast to Si homoepitaxy where there are “denuded zones” within a characteristic distance of the S_B steps.^{16,17} This emphasizes the importance of step edges while suggesting that they play a minor role in the formation of regrowth structures.

In Figs. 1(a) and 1(b) we have identified bright features, labeled *X*, that are observed after etching at 600 K. These features appear less frequently at 700 K, and are seen rarely at 800 K or higher. While STM cannot establish their chemical identity, we propose that they represent silicon bromide species that were unable to desorb because of the relatively low temperature. This is consistent with TPD analysis⁸ that associated the α state with highly-coordinated species like SiBr_4 . Such species desorb in the range ~ 400 –700 K and the *X* features could be due to molecules that had not yet desorbed. Alternatively, they could reflect the Br-poor species of the β state that are not sufficiently volatile to desorb completely.

Steady-state surfaces such as those in Fig. 1 with small etch pits and rough steps are consistent with TPD results that indicate that the α state corresponds to highly-

coordinated SiBr_x species which are more easily created at exposed steps. We conclude that etching occurs primarily at step edges, supplemented by limited etching at native terrace defects where Si-Si bonds may be more easily broken than on pristine terraces. Accordingly, continuous etching results in step retreat that is analogous to step flow in growth. Low yield etching at step edges allows local healing through atomic rearrangement and incorporation of diffusing species. This prevents severe roughening of step profiles.

C. Intermediate-temperature (IT) etching at 800 and 900 K

Comparison of the images in Figs. 1 and 2 demonstrates a dramatic change in the steady state morphology when the temperature exceeds ~ 750 K, the desorption threshold for the β state. Images from surfaces etched at 800 K show more local height variation because etch pits and islands constitute $\sim 30\%$ of the area of terraces. At 800 K, these features are larger and exhibit increased shape anisotropies. Anisotropic etching from etch pits into surrounding terraces and from intrinsic steps reflects weakened Si-Si back bonds and increased volatility of the lower SiBr_x species. An increase in step roughness at 800 K is apparent by comparing Fig. 2(b) with an equivalent step etched at 700 K in Fig. 1(c). Increased roughness results from a combination of thermally enhanced etching into the terrace and the regrowth of free Si near the step edge. Hence, etching at 800 K can be characterized as the creation and growth of single-layer etch pits on terraces as a complement to step etching.

In discussing the morphology for surfaces etched at 800 K, it is important to identify whether the terrace islands result from regrowth or whether they represent remnants of terrace etching. Several observations lead to the conclusion that many are remnants and that these remnants serve as sites for accommodation of mobile Si. First, measurements after exposure > 3 mA sec at 800 K indicate that the total area of the terrace islands exceeds that of the terrace etch pits [Figs. 2(a) and 2(b)]. Since the ratio of island area to pit area on a given terrace remains constant at ~ 1.5 , it is clear that all of the Si atoms ejected from pits could not account for the islands, even if no desorption of volatile species were to occur. Second, while step etching contributes Si atoms, the ratio of island area to pit area is the same near and far from steps. The diffusion length on heavily pitted terraces is likely to be small because pits can act as sinks to diffusing species. Thus, regrowth structures derived from atoms released from step edges would be concentrated near steps. Finally, annealing a surface like Fig. 2(a) for ~ 1 h at 800 K did not eliminate the chains and islands from the terraces, although they did become fragmented due to additional desorption of SiBr_x . This implies that they are relatively stable at 800 K, making it unlikely they originated as pure regrowth structures.

While the islands are stable, the absence of antiphase boundaries within extended pits indicates that there is sufficient thermal energy that independent 2×1 domains can reconstruct to avoid boundary formation. Such boundary development would be expected for etch pits

that nucleate independently on an open terrace and subsequently grow together. The absence of domain boundaries after etch pits coalescence is similar to what has been observed for high-temperature homoepitaxial growth of Si on Si(100).¹²

The remnant islands become fragmented and the Si atoms are incorporated at pit and step edges as the area of the dominant terrace decreases due to etch pit expansion and coalescence. Significantly, these islands remain two-dimensional rather than evolving into rough, three-dimensional structures, and no more than three layers are exposed on a given terrace. Three-dimensional roughening is inhibited because a given layer will etch preferentially along the dimer row direction and this direction alternates from one layer to the next. Second-layer etching is then confined by the smaller dimension in the first layer. Therefore, we conclude that etching at 800 K is governed by the nucleation and growth of etch pits in a layer-by-layer fashion.

Figure 2(c) shows that the dominant terraces on steady-state surfaces at 900 K consist of numerous small etch pits and mixed 2×1 and 3×1 domains. High-resolution images show that the 3×1 domains are composed of Si dimer rows separated by missing atom rows.¹⁸ Two-dimensional patches exist on these terraces that also contain 2×1 and 3×1 domains. The evolution of this patterned surface as a function of flux and fluence during continuous etching at 900 K has been described elsewhere.^{6,7,18} Briefly, 3×1 patterning requires a sufficient local concentration of Br and temperatures in the range ~ 850 –900 K.¹⁸ The conversion of Br-terminated 2×1 domains to 3×1 domains requires the coordinated breaking of dimer bonds with redimerization that produces SiBr_2 rows between Br-terminated Si dimer rows.¹⁸ The volatile SiBr_2 rows are unstable against desorption and their departure leaves rows of Br-terminated dimers separated by missing atom rows. We note that isolated 3×1 structures have been observed for etching at other temperatures and also in Si homoepitaxy. Their absence as extended domains in these cases emphasizes the restricted conditions under which patterning occurs. While some 2×1 islands due to standard regrowth processes are found after etching at 900 K, it is clear that the dominant 3×1 morphology results from this specific mechanism.

D. High-temperature (HT) etching at 1000 and 1100 K

Exposure of Si(100)- 2×1 to Br_2 at 1000 and 1100 K results in steady-state etching that is characterized by scattered small pits and patches of clean Si among Br-terminated areas, as shown in Figs. 3(a) and 3(b). The Br-free Si dimers, labeled Si, can be differentiated from Br-terminated dimers, labeled Br, because they are brighter at a sample bias voltage of approximately -1 V.⁷ The ability to distinguish between the two types of sites makes it possible to conclude that approximately half of the surface is Br free even after extended Br_2 exposure and etching at 1000 K [Fig. 3(a)]. Images obtained after etching at 1100 K show that there is almost no residual Br [Fig. 3(b)]. These results are consistent with TPD data that reveal complete desorption after heating

brominated surfaces to 1100 K.⁸ Inspection also shows disorder in the bright structureless features labeled *Y* in Figs. 3 and 4(b). Often collected in roughly linear patterns, these features could represent amorphous Si structures and halogenated species where ordering has been frustrated by the disruption of the terrace.

The large-scale image of Fig. 4(a) reveals the morphology of a surface etched to steady state at 1000 K. For this surface, the original terraces were $\sim 0.3\text{--}0.4\ \mu\text{m}$ wide and the steps ran from the upper left to the lower right. After etching, the original step configuration was not readily identifiable. Etching exposed five layers, labeled *A–E* where *C* represents the dominant layer. Residual strands of layer *A* occupy the larger islands of layer *B*. Large pits (*P1*) are formed in *C* with dimensions of $\sim 0.1\ \mu\text{m}$. Within them are smaller pits (*P2*) with dimensions of $\sim 100\ \text{Å}$. Again, the pits are anisotropic and no antiphase domain boundaries could be detected within the pits. The steps at the pit perimeters, however, are ragged and the pits themselves are less rectilinear than those produced at lower temperatures.

Multilayer etching is established at fluences as low as 1.6 mA sec at 1000 K. It represents the steady-state condition for surfaces having $0.3\text{--}0.4\text{-}\mu\text{m}$ -wide terraces. For samples with narrow terraces ($\sim 200\ \text{Å}$ wide), however, only three layers are exposed on a given terrace. The difference can be understood by again noting that a pit is elongated along the dimer row direction on a given terrace. Large terraces allow wider pits to form, pits that can grow to appreciable size are ultimately formed in the next exposed layer, and so forth. Again, steady-state morphology will reflect bounded roughening, even for etching on surfaces with low miscut.

Etching at 1000 K can be characterized by a process where weakened Si-Si bonds and enhanced Br diffusion combine to promote facile step etching. At the same time, terrace defect creation is also more likely, and these defects can rapidly expand, ultimately coalescing to create large pits. These processes expose several layers, the number of which depends on the kinetics and the terrace width. Multilayer etching is inhibited at lower temperatures by reduced terrace attack.

Etching at 1100 K results in a distinct morphology because of increased reactivity, lower residence time of Br on the surface, and higher vacancy mobility. In particular, imperfect line defects (LD) appear that run perpendicular to the dimer rows. There are also irregularly shaped single-layer pits (*P*) that are distributed throughout the network of line defects [Figs. 3(b) and 4(b)]. Following the morphology from the initial stages of etching offers insight into LD formation because low fluences create randomly distributed missing dimer effects and small pits, and the local defect morphology appears much like that for etching at 1000 K [Fig. 3(a)]. Annealing at this stage at 1100 K without additional Br₂ exposure for ~ 15 min orders these isolated defects into line defects, demonstrating their mobility. The average defect length increases with continued exposure at 1100 K and the average spacing decreases so that the surface evolves into a steady-state $2\times n$ network of line defects where $6\leq n\leq 12$. The line defects are then $25\text{--}50\ \text{Å}$ apart and

individual defects can reach lengths of ~ 30 dimer rows. Flashing a sample that has reached the configuration shown in Figs. 3(b) and 4(b) results in a lower defect density. We conclude that line defect nucleation requires a minimum vacancy density and sufficient time at high temperature for diffusion processes to organize the vacancies into lines. (We also note that annealing a clean surface at 1100 K did not result in line defect formation so it is established that metal contamination¹⁹ plays no role in line defect formation in our experiments.)

Zandvliet and co-workers^{20,21} have reported line defect formation on ion sputtered Si(100)- 2×1 after annealing at 875–1125 K, showing STM images that were similar to Figs. 3(b) and 4(b). Significantly, we observe a large number of vacancies but few defects for etching at 1000 K. This suggests that the surface concentration of Br affects vacancy diffusion. In the context of the wave like vacancy diffusion model proposed by Zhang, Chen, Bolding, and Lagally,²² Br chemisorbed to dimer dangling bonds could inhibit vacancy diffusion, thereby preventing the formation of line defects. Support for this assertion comes from post-etch annealing of surfaces exposed to Br₂ at 1000 K: Line defects formed and Br disappeared from the surface after heating to 1000 K for 5 min without a Br₂ flux. In addition, once the Br was desorbed, there was sufficient Si mobility at 1000 K that the etch damage healed and the surface returned to a regularly stepped morphology.

Si 2×1 DIMER CHAINS

In the following, we consider chain formation associated with steady-state etching between 700 and 900 K. The formation of dimer chains and two-dimensional islands can be compared to the formation of such structures during Si homoepitaxy on Si(100).^{12–14} Although homoepitaxial growth favors Si accommodation at *S_B* steps and the development of denuded zones near *S_B* steps,^{16,17} we find no such denuded zones. Since denuded zones are a consequence of anisotropic surface diffusion, their absence on pitted and Br-bonded surfaces indicates different diffusion characteristics. Moreover, step etching may counteract the tendency to form denuded zones by liberating Si for local regrowth.

Figure 5(a) shows several dimer chains and several etch pits on a surface etched at 800 K. The chains run perpendicular to the terrace dimer rows. Within a chain the bright elliptical features are individual dimers. At the ends of chains, the dimers appear brighter, most likely due to a slight relaxation. Examples of chains with even (*E*) and odd (*O*) numbers of dimers are labeled. Extensive counting demonstrates that chains with an odd number of dimers greatly outnumber those with an even number for etching between 700 and 900 K. Significantly, most even-length chains appear in pairs (EP) separated by a single missing dimer. This suggests that they are segments of odd-length chains that were split.

Removal of a dimer from an odd-length chain could produce either two even-length segments or two odd-length segments, as depicted in Fig. 5(b). The schematic

shows a 2×1 -reconstructed terrace layer (filled circles) with three-odd-length dimer chains (open circles) that have lost one dimer. Removal from the site, labeled *R*, equivalent to one atop a dimer row of the terrace, results in odd-length pair segments (OP), shown on the right side of Fig. 5(b). Removal from the trough site *T* results in even-length pair segments (EP), depicted in the center of the figure. Removal from the end of an odd-length chain creates an isolated even-length (*E*) chain. Analysis of many images like Fig. 5(a) revealed nearly equal numbers of EP and OP segments, demonstrating that neither the trough nor the row sites were preferentially vacated. Finally, odd length chains with end dimers that were both atop rows of the underlying terrace were rare. We find that only $\sim 5\%$ of the chains are of the isolated even-number type after etching at 700 and 800 K. (To arrive at this number, we counted EP and OP chains as longer

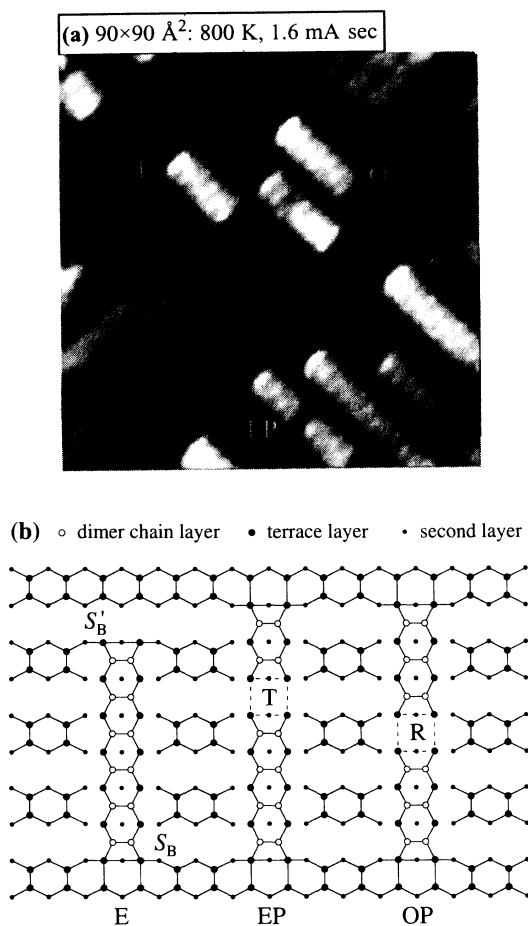


FIG. 5. (a) Occupied states image showing even- and odd-numbered dimer chains, *E* and *O*, respectively. Chain termination is favored in the troughs between dimer rows of the underlying terrace, resulting in odd-length (*O*) chains. Other structures such as even-length paired segments (EP) separated by a single missing dimer are thought to originate as odd-length chains. (b) Schematic showing rebonded S_B and nonbonded S'_B steps. Configurations for even- and odd-length paired segments (EP and OP) are shown to result from removal of dimers that were atop troughs (*T*) or dimer rows (*R*) of the underlying terrace.

odd-length chains.) For a 3×1 steady-state surface produced at 900 K, the fraction of even-length chains increased to $\sim 10\%$. The increase can be attributed to the coordinated etch mechanism responsible for 3×1 domain formation. In particular, these dimer chains do not develop via standard growth processes of the sort reflected by etching at 700 and 800 K and there is greater terrace fragmentation at 900 K.

The dominance of odd-length chains is explained by the energetics of step formation. A dimer chain is terminated at either end by local structures that resemble *B*-type steps. There are two kinds of *B*-type steps, as depicted at the left of Fig. 5(b). "Rebonded" S_B steps are energetically favored over "nonbonded" or S'_B steps where the bonding configurations refer to terrace-layer atoms.²³ For S_B steps, the atoms on the terrace have all four bonds satisfied. However, an S'_B step leaves the second-layer atoms with one dangling bond each, increasing the number of dangling bonds by two. This is energetically unfavorable.²³ The preference for rebonded S_B steps is reflected at step edges on clean Si(100)- 2×1 where kinks in S_B steps are nearly always an even number of dimers long.^{16,24} Here, we see that the dimer chains preferentially begin and end with dimers situated above the trough between dimer rows of the terrace below, forming S_B steps. This type of structure requires an odd number of dimers.

Statistical distributions for odd length chains are shown in Fig. 6 for steady-state etching at 700, 800, and

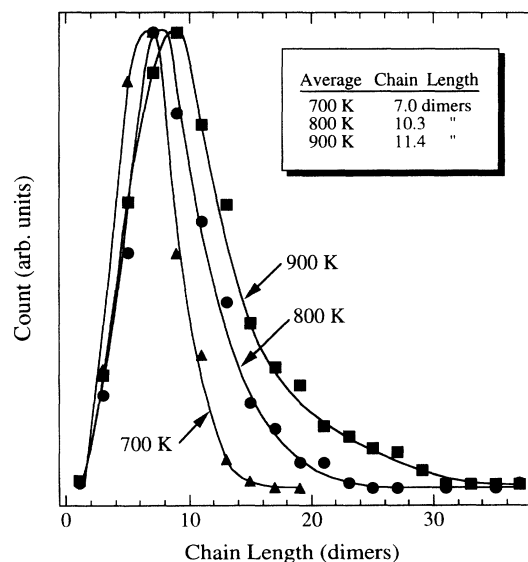


FIG. 6. Dimer chain length distributions for steady-state surfaces etched at 700, 800, and 900 K. The distributions broaden and shift with increasing temperature, resulting in longer average chain lengths. Chain lengths are dependent on the amount of Si available for growth and this increases with temperature. Chain lengths also depend on the growth mechanism. It is pure regrowth at 700 K and regrowth on existing chains at 800 K. At 900 K, the distribution exhibits a long-length tail due to the creation of 3×1 domains consisting of dimer rows separated by missing atom rows. Here the chain length is limited by domain size.

900 K. Chains that were incorporated into islands wider than two dimer rows were not included in the analysis to minimize the influence of large islands on the nucleation, growth, and coarsening of dimer chains. The distributions have been normalized to their peak values for comparison. Chains for the 900 K case were predominantly from 3×1 domains which cover much of the steady-state surface, while those from surfaces etched at 700 and 800 K were from 2×1 domains. A shift of the peaks in Fig. 6 to greater length with increasing temperature is evident, and the tails of the distributions represent increasing fractions of the total count. The shifts and the broadenings translate into longer average chain lengths or higher shape anisotropies. The average lengths are reported in the inset of Fig. 6.

Factors contributing to dimer chain lengths include temperature-dependent effects such as the amount of material available for regrowth, the method of their formation, and the average distance between etch pits. The length of chains on surfaces etched at 700 K is limited by the amount of material available for regrowth. For surfaces etched at 800 K, however, the chain length is limited by the distance between etch pits. The increase in chain length from 700 to 800 K can be attributed primarily to extra material for regrowth at 800 K where the desorption threshold for SiBr_2 is exceeded. For etching up to 800 K, a larger amount of Si is liberated with increasing temperature, and this counteracts the tendency of coarsening and etching to shorten the chains. At 900 K, chain formation relies on the spontaneous etch process that creates 3×1 domains from 2×1 terraces. Therefore, the chain length is limited by the domain size.

CONCLUSIONS

We have determined the dependence of the surface morphology on temperature for Br-etched $\text{Si}(100)-2 \times 1$, as summarized in Fig. 7. The morphologies reflect temperature-dependent etch product evolution, diffusion, and surface reactivity. Material removal was found to proceed via step retreat or layer-by-layer etching in all cases, resulting in bounded surface roughness. The dom-

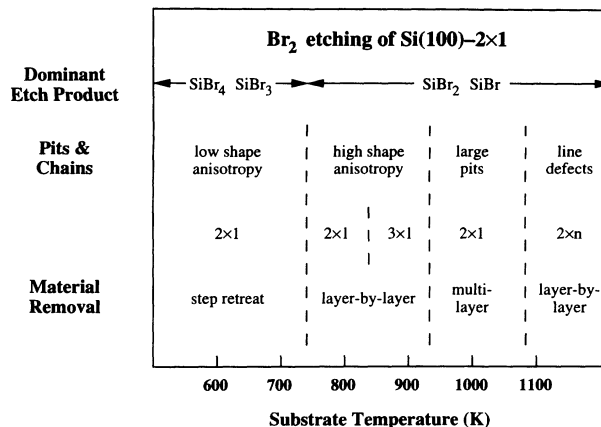


FIG. 7. Schematic summary of temperature-dependent morphologies resulting from Br_2 etching of $\text{Si}(100)-2 \times 1$. Transitions from one region to another are gradual and only the dominant behavior is given.

inant surface reconstruction was 2×1 except for the special case of etching at 900 K where small 3×1 domains were produced. Line defects were observed after etching at 1100 K and these gave rise to a weak $2 \times n$ reconstruction.

These studies have emphasized temperature-dependent morphologies associated with $\text{Si}(100)-2 \times 1$ with large terraces and single height steps. It will remain for further work to examine differences that might be related to the reactivity of double height steps and to extend the parameter space beyond flux, fluence, and temperature. In the framework of the latter, it will be very important to examine simultaneous exposure to a halogen etchant and an energetic ion beam or to examine the effects of ionized halogens having appreciable kinetic energies.

ACKNOWLEDGMENTS

This work was supported by the Office of Naval Research. The authors thank X.-S. Wang for discussion and technical assistance.

¹R. J. Schutz, in *VLSI Technology*, edited by S. M. Sze (McGraw-Hill, New York, 1988), p. 184.

²H. F. Winters and J. W. Coburn, *Surf. Sci. Rep.* **14**, 161 (1992).

³J. C. Patrin, Y. Z. Li, M. Chander, and J. H. Weaver, *Appl. Phys. Lett.* **62**, 1277 (1993).

⁴J. C. Patrin and J. H. Weaver, *Phys. Rev. B* **48**, 17913 (1993).

⁵J. J. Boland and J. S. Villarrubia, *Science* **248**, 838 (1990).

⁶M. Chander, Y. Z. Li, J. C. Patrin, and J. H. Weaver, *Phys. Rev. B* **47**, 13035 (1993).

⁷D. Rioux, M. Chander, Y. Z. Li, J. C. Patrin, and J. H. Weaver, *Phys. Rev. B* **49**, 11071 (1994).

⁸R. B. Jackman, R. J. Price, and J. S. Foord, *Appl. Surf. Sci.* **36**, 296 (1989).

⁹B. S. Swartzentruber, Y.-W. Mo, M. B. Webb, and M. G. Lagally, *J. Vac. Sci. Technol. A* **7**, 2901 (1989).

¹⁰N. D. Spencer, P. J. Goddard, P. W. Davies, M. Kitson, and R. M. Lambert, *J. Vac. Sci. Technol. A* **1**, 1554 (1983).

¹¹R. J. Hamers, R. M. Tromp, and J. E. Demuth, *Phys. Rev. B* **34**, 5343 (1986).

¹²R. J. Hamers, U. K. Köhler, and J. E. Demuth, *Ultramicroscopy* **31**, 10 (1989).

¹³J. Y. Tsao, E. Chason, U. Koehler, and R. Hamers, *Phys. Rev. B* **40**, 11951 (1989).

¹⁴Y.-W. Mo, B. Swartzentruber, R. Kariotis, M. B. Webb, and M. G. Lagally, *Phys. Rev. Lett.* **63**, 2393 (1989).

¹⁵R. J. Hamers, P. Avouris, and F. Bozso, *Phys. Rev. Lett.* **59**, 2071 (1987).

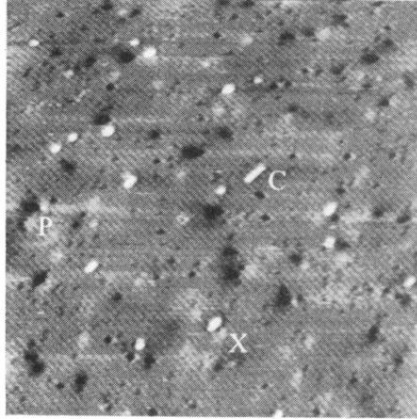
¹⁶C. Roland and G. H. Gilmer, *Phys. Rev. B* **46**, 13437 (1992).

¹⁷Y.-W. Mo and M. G. Lagally, *Surf. Sci.* **248**, 313 (1991).

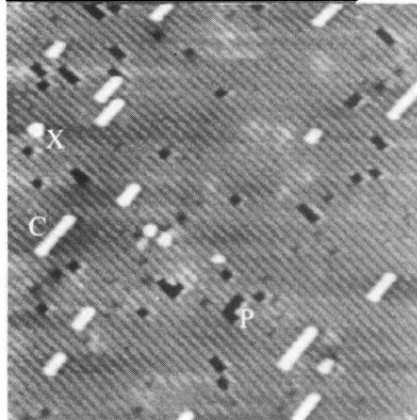
¹⁸M. Chander, Y. Z. Li, D. Rioux, and J. H. Weaver, *Phys. Rev.*

- Lett. **71**, 4154 (1993).
- ¹⁹H. Niehus, U. K. Koehler, M. Copel, and J. E. Demuth, *J. Microsc.* **152**, 735 (1988).
- ²⁰H. Feil, H. J. W. Zandvliet, H.-H. Tasi, J. D. Dow, and I. S. T. Tsong, *Phys. Rev. Lett.* **69**, 3076 (1992).
- ²¹H. J. W. Zandvliet, H. B. Elswijk, E. J. van Loenen, and I. S. Tsong, *Phys. Rev. B* **46**, 7581 (1992).
- ²²Z. Zhang, H. Chen, B. C. Bolding, and M. G. Lagally, *Phys. Rev. Lett.* **71**, 3677 (1993).
- ²³J. Chadi, *Phys. Rev. Lett.* **59**, 1691 (1987).
- ²⁴B. S. Swartzentruber, Y.-W. Mo, R. Kariotis, M. G. Lagally, and M. B. Webb, *Phys. Rev. Lett.* **65**, 1913 (1990).

(a) $575 \times 575 \text{ \AA}^2$: 600 K, 9.6 mA sec



(b) $380 \times 380 \text{ \AA}^2$: 700 K, 7.2 mA sec



(c) $700 \times 700 \text{ \AA}^2$: 700 K, 7.2 mA sec

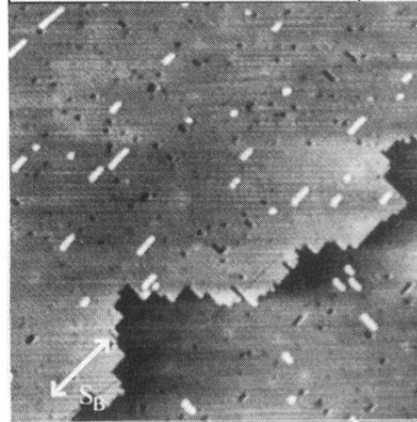
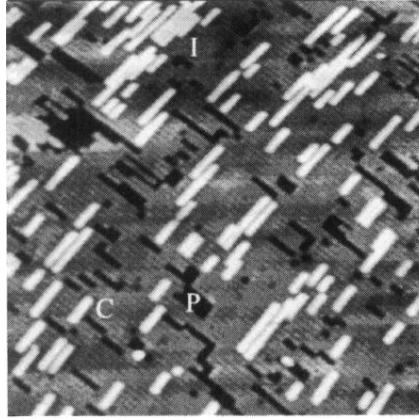
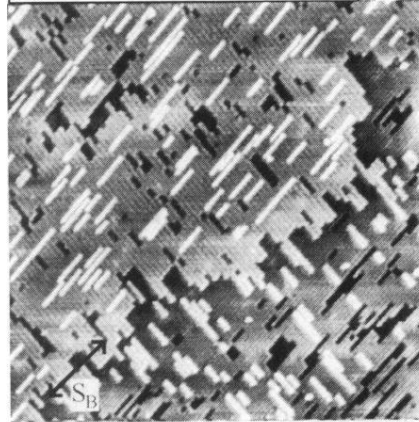


FIG. 1. Occupied states images of Si(100)- 2×1 exposed to Br_2 at (a) 600 K and (b), (c) 700 K. The images represent steady-state conditions in that they do not change in overall appearance with further exposure. The number and size of dimer chains (C) and anisotropic single-layer etch pits (P) increase with increasing temperature. The bright structureless features (X) may represent nonvolatile silicon bromide species. In (c) an S_B step edge crosses the image. Analysis indicates that such steps are roughened during etching but the terraces remain relatively defect free. Hence, etching is dominated by a step flow mechanism at 600 and 700 K. In this temperature region, desorption species are predominantly SiBr_3 and SiBr_4 .

(a) $460 \times 460 \text{ \AA}^2$: 800 K, 7.2 mA sec



(b) $550 \times 550 \text{ \AA}^2$: 800 K, 7.2 mA sec



(c) $600 \times 600 \text{ \AA}^2$: 900 K, 7.2 mA sec

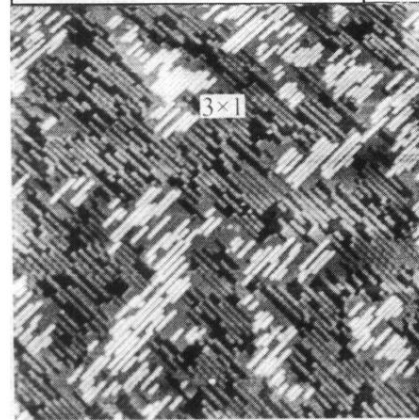


FIG. 2. Occupied states images of Si(100)- 2×1 exposed to Br_2 at (a), (b) 800 K and (c) 900 K. At 800 K a pathway involving SiBr_2 desorption is activated and this increases the etch rate. The result is enhanced terrace etching and rougher step edges. Step roughening occurs through facile material removal and Si regrowth near step edges. Etching also proceeds by pit formation on terraces at 800 K. As pits expand and coalesce, remnants of the terrace create islands that nucleate regrowth. At 900 K, 3×1 domains are produced by a coordinated surface transformation that yields atom rows of SiBr_2 separated by Br-terminated dimer rows. The SiBr_2 rows are volatile and desorb spontaneously, leaving behind dimer rows separated by missing atom rows [see text].

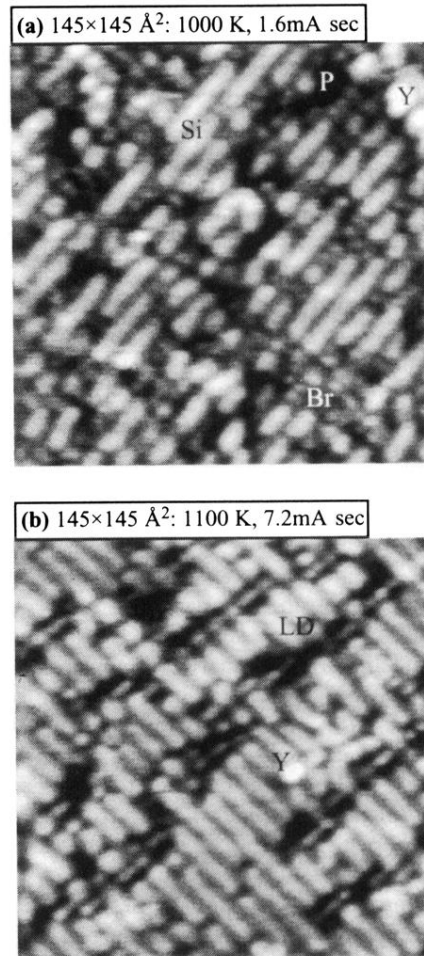


FIG. 3. Small-scale images taken after steady-state etching at (a) 1000 K and (b) 1100 K. (a) shows Br-free Si dimers (Si) and Br adsorption sites (Br) that are mixed with irregularly shaped pits (P). The bright feature labeled Y represents a disordered regrowth structure. (b) Dimer vacancies interact to form line defects (LD) that run perpendicular to the dimer row direction. Very little Br remains after etching at 1100 K and quenching to room temperature for imaging.

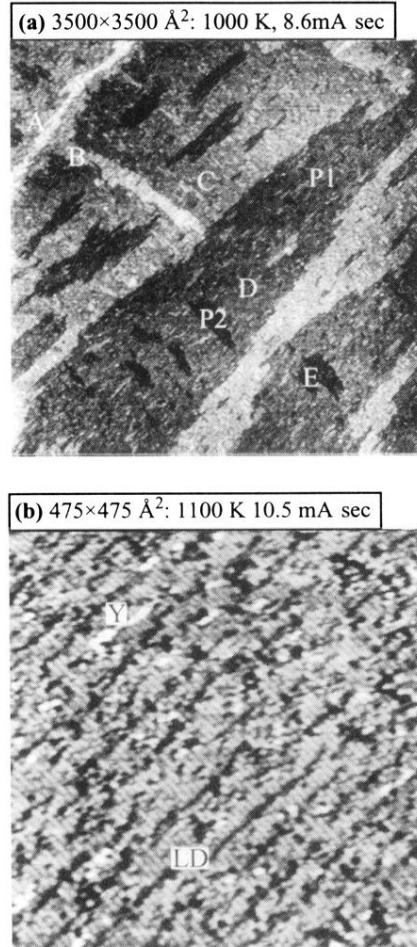
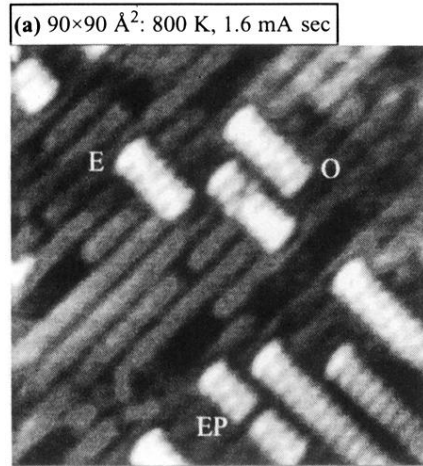


FIG. 4. Large-scale images taken after etching at (a) 1000 K and (b) 1100 K. (a) Five layers of Si are exposed by steady-state etching of a surface with $0.3\text{--}0.4\text{-}\mu\text{m}$ -wide terraces. Layers *A* and *B* are largely removed. Layer *C* dominates but large pits (*P1*) expose layer *D* and smaller pits (*P2*) expose layer *E*. This roughening is due to weakened Si-Si bonds and enhanced diffusion of Br. Surface defects are readily created and they facilitate terrace etching. (b) Etching at 1100 K produces a large number of vacancy defects. These defects are sufficiently mobile that they form networks of line defects. Roughly linear collections of bright features (*Y*) on terraces resemble regrowth structures, but the terrace disruption prevents the creation of ordered structures.



(b) \circ dimer chain layer \bullet terrace layer \cdot second layer

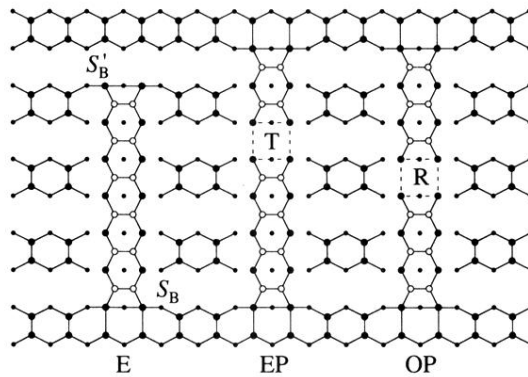


FIG. 5. (a) Occupied states image showing even- and odd-numbered dimer chains, E and O , respectively. Chain termination is favored in the troughs between dimer rows of the underlying terrace, resulting in odd-length (O) chains. Other structures such as even-length paired segments (EP) separated by a single missing dimer are thought to originate as odd-length chains. (b) Schematic showing rebonded S_B and nonbonded S'_B steps. Configurations for even- and odd-length paired segments (EP and OP) are shown to result from removal of dimers that were atop troughs (T) or dimer rows (R) of the underlying terrace.